Band structure of two-dimensional photonic crystals that include dispersive left-handed materials and dielectrics in the unit cell

Alberto Mendoza-Suárez,[1] Francisco Villa-Villa,[2,*] and Jorge A. Gaspar-Armenta[3]

[1]*Facultad de Ciencias Físico-Matemáticas, Universidad Michoacana de San Nicolás de Hidalgo, Edificio "B," Ciudad Universitaria 58060, Morelia, Michoacán, México*
[2]*Centro de Investigaciones en Optica, Loma del Bosque 115, Lomas del Campestre, León Gto. 37150, México*
[3]*Centro de Investigación en Física de la Universidad de Sonora, Apdo. Post. 5-088, Hermosillo Sonora 83190, México*
[*]*Corresponding author: fvilla@cio.mx*

Received July 16, 2007; revised October 17, 2007; accepted October 18, 2007; posted October 29, 2007 (Doc. ID 85301); published November 30, 2007

We determine the band structure of two-dimensional photonic crystals that are composed of left-handed materials and dielectrics, based on the numerical solution of the Helmholtz equation by using integral equations. It is found that plasmonic resonances appear constituting a band that is independent of the filling fraction. Wide bandgaps are present where the penetration depth of the electromagnetic field inside the photonic crystal is quite short compared to purely dielectric photonic crystals. © 2007 Optical Society of America

OCIS codes: 290.0290, 240.6690.

1. INTRODUCTION

Photonic crystals that constitute periodic arrays of different materials in one, two, and three dimensions with unit cells whose magnitude is on the order of the wavelength of the light are the subject of much research in recent years because of their potential to develop completely optical integrated circuits [1–7].

It has been proved in the past several years that adding new materials to the structure of photonic crystals results in novel properties of these systems that were originally conceived as composed of purely dielectric materials. Some of the more interesting properties present in these systems are light confinement [8], waveguiding [5–7], negative refraction [9], high refraction through the superprism effect [10,11], and signal commutation by including defects of nonlinear materials [12]. Quite recently a light controlled commuting device has been obtained that has a response on the order of picoseconds [1].

Other kinds of structured materials that have recently attracted much interest are the left-handed materials (LHMs), which owe their name to the fact that the light vectors $\vec{E}$, $\vec{H}$, and $\vec{k}$ form a left-handed triad for a wave propagating through these media. LHM were first designed as periodic arrays of metallic capacitors and wires with a unit cell of dimensions much smaller than the wavelength. Although fundamental experiments with LHMs have been developed for the microwave region of the electromagnetic spectrum [13], promising theoretical results exist indicating that LHM will be available soon for the visible region of the spectrum by the use of nanotechnology [14].

In recent theoretical studies it also has been found that including LHM into the unit cell of one-dimensional photonic crystals can drastically change their band structure [15–17], producing interface mode bands that are not present in completely dielectric systems [18]. Also a tunnel effect appears in the middle of some bandgaps that is a consequence of the fact that the total optical path sums zero phase retardation under certain conditions. Brewster points that produce narrowing and closing of bandgaps could also appear in both polarizations [19].

In this context, the present work is concerned with determination of the optical response and band structure of two-dimensional photonic crystals that include LHMs and dielectrics (LR2DPC) by applying a numerical method based on Green's second identity to solve the Helmholtz equation.

2. THEORY

Assuming a sinusoidal time dependence $e^{-i\omega t}$ for the electromagnetic fields, the wave equation can be transformed to the Helmholtz equation:

$$\nabla^2\Psi_j(\vec{r}) + k_j^2\Psi_j(\vec{r}) = 0. \tag{1}$$

In this equation $\Psi_j(\vec{r})$ represents the electric field E_z in the case of TE polarization, and the magnetic field H_z in the case of TM polarization, both in the jth medium (Fig. 1). The magnitude of the wave vector is given by

$$k_j = n_j(\omega)\frac{\omega}{c}, \tag{2}$$

where the refractive index $n_j(\omega) = \pm\sqrt{\mu_j(\omega)\varepsilon_j(\omega)}$ that involves the material's properties is given in terms of the magnetic permeability $\mu_j(\omega)$ and the electric permittivity is given by $\varepsilon_j(\omega)$, both of these functions depending on the frequency ω. The speed of light is indicated by c. The sign appearing in the refractive index equation must be taken

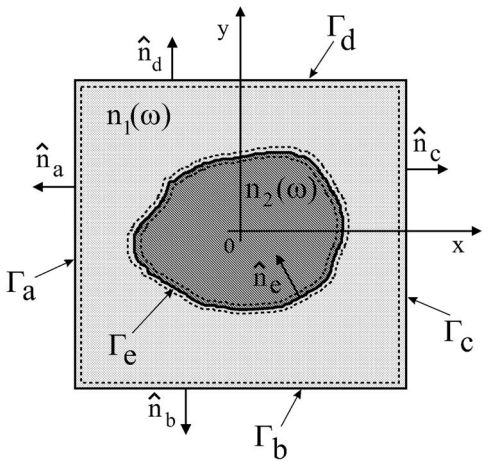

Fig. 1. Unit cell of a 2DPC composed of two different materials with refractive indices $n_1(\omega)$ and $n_2(\omega)$. The two different regions are limited by the contours $\Gamma_a, \Gamma_b, \ldots, \Gamma_e$, whose normal vectors are given in the figure. Dashed curves represent closed contours inside each medium.

as negative when considering an LHM and positive when the medium is a dielectric material.

With LR2DPC, the position vector $\vec{r}$ will be a two-dimensional vector in the x–y plane, since we are assuming a periodic array of rods of square or circular section that are infinitely long with their symmetry axis aligned with the z axis. For brevity we will use the term unit cell with square or circular inclusion, although it is possible to consider a transversal section of arbitrary shape.

Let us now consider the equation involving the Green's function $G_j(\vec{r},\vec{r}')$,

$$\nabla^2 G_j(\vec{r},\vec{r}') + k_j^2 G_j(\vec{r},\vec{r}') = -4\pi\delta(\vec{r}-\vec{r}'), \tag{3}$$

where $\delta(\vec{r}-\vec{r}\,')$ is the Dirac delta function. In our problem, which has cylindrical symmetry (electromagnetic field independent of z), a useful Green's function can be represented by

$$G_j(\vec{r},\vec{r}') = i\pi H_0^{(1)}(k_j|\vec{r}-\vec{r}'|), \tag{4}$$

where $H_0^{(1)}(\zeta)$ is a Hankel function of the first kind and order zero [20–22].

By applying the two-dimensional Green's second integral theorem to $\Psi_j(\vec{r}')$ and $G_j(\vec{r},\vec{r}')$ for each region corresponding to the jth medium, we have [20]

$$\int_{S_j} \delta(\vec{r}'-\vec{r})\Psi_j(\vec{r}')\mathrm{d}A' = \frac{1}{4\pi}\oint_{C_j}\left[G_j(\vec{r},\vec{r}')\frac{\partial\Psi_j(\vec{r}')}{\partial n'_j} - \frac{\partial G_j(\vec{r},\vec{r}')}{\partial n'_j}\Psi_j(\vec{r}')\right]\mathrm{d}s'. \tag{5}$$

In this equation, the surface S_j is limited by the corresponding closed contour C_j, and $\partial/\partial n_j$ is the derivative along the outward normal to contour C_j. The contours present in the unit cell are $C_1=\Gamma_a+\Gamma_b+\Gamma_c+\Gamma_d+\Gamma_e$ and $C_2=\Gamma_e$ (see Fig. 1). From Eq. (5) a set of coupled integral equations for Ψ_j and $\partial\Psi_j/\partial n_j$ can be obtained, evaluating $\vec{r}$ in the vicinity of the contours.

The geometry of the problem is described by representing the points of the profiles with Cartesian coordinates,

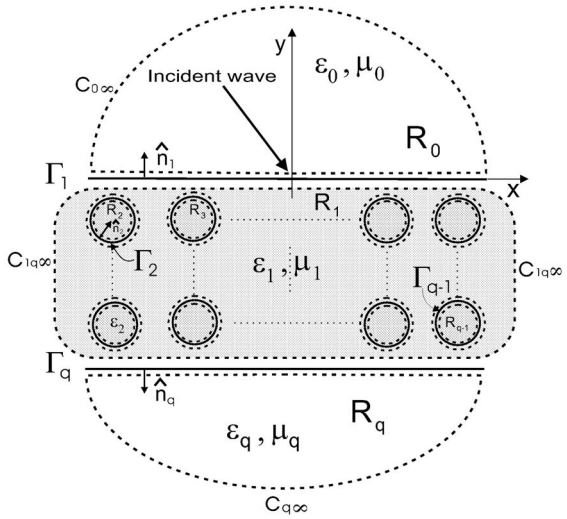

Fig. 2. Scheme of a finite LR2DPC. The integration contours are indicated in dashed curves. R_0 and R_q represent the regions enclosing the incident and transmission media, respectively.

$X(s)$, $Y(s)$, as parametric functions of the arc length s, and their derivatives $X'(s)$, $Y'(s)$, $X''(s)$, and $Y''(s)$ up to the second order. These parametric functions are numerically generated by sampling the profiles $\Gamma_a, \Gamma_b, \ldots, \Gamma_e$, by the position vectors,

$$\vec{R}_{n(q)} = (X_{n(q)}, Y_{n(q)}) = [X(s_{n(q)}), Y(s_{n(q)})], \tag{6}$$

where $q=a,b,\ldots,e$ is used to denote the different integration paths $\Gamma_a, \Gamma_b, \ldots, \Gamma_e$, and $n=1,2,\ldots,N_q$ denotes their corresponding points resulting from a given partition. We called N_q the number of points taken along the corresponding contour Γ_q. Then, we have a total of $N_a+N_b+N_c+N_d+N_e$ sampling points.

The discrete approximations of the two different terms appearing in Eq. (5) are [20–22]

$$\frac{1}{4\pi}\int_{\Gamma_q}\Psi_j(\vec{r}')\frac{\partial G_j(\vec{r},\vec{r}')}{\partial n'}\mathrm{d}s' \cong \sum_{n=1}^{N_q} N^{(j)}_{mn(q)}\psi^{(j)}_{n(q)}, \tag{7}$$

$$\frac{1}{4\pi}\int_{\Gamma_q} G_j(\vec{r},\vec{r}')\frac{\partial\Psi_j(\vec{r}')}{\partial n'}\mathrm{d}s' \cong \sum_{n=1}^{N_q} L^{(j)}_{mn(q)}\Phi^{(j)}_{n(q)}, \tag{8}$$

where $\Psi^{(j)}_{n(q)} = \psi_j(\vec{r}')|_{\vec{r}'=\vec{R}_{n(q)}}$ indicates the fields and

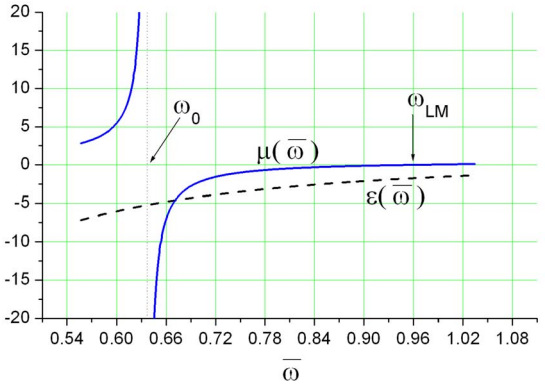

Fig. 3. (Color online) Dielectric function and magnetic permeability of a dispersive LHM as a function of frequency.

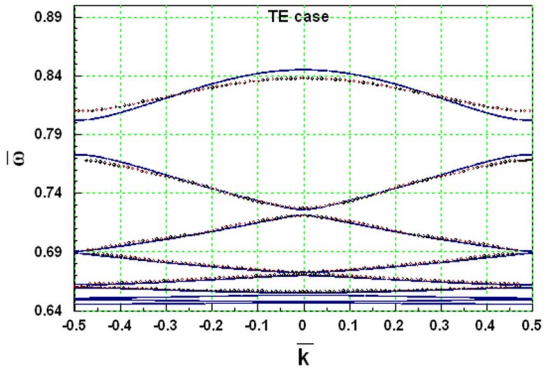

Fig. 4. (Color online) Band structure under TE polarization and normal incidence ($\bar{\beta}=0$) for a 1DPC whose unit cell is composed of two materials, vacuum (n_1) and a LHM (n_2), with $d_1=0.3D$, $d_2=0.7D$. Solid curves indicate the results obtained with the proposed method, while dashed curves correspond to results obtained by the characteristic matrix method.

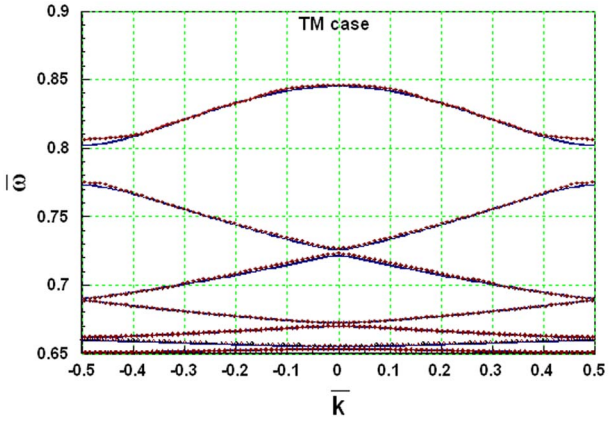

Fig. 5. (Color online) Band structure under TM polarization. Same parameters as the previous figure.

$$\Phi_{n(q)}^{(j)} = \left.\frac{\partial \psi_j(\vec{r}')}{\partial n'_j}\right|_{\vec{r}'=\vec{R}_{n(q)}},$$

their corresponding normal derivatives. m indicates the mth point [observer's coordinates $\vec{r}=(x_m,y_m)$] along the contour Γ_p with $p=a,b,\ldots,e$. The matrix elements, $L_{mn(q)}^{(j)}$ and $N_{mn(q)}^{(j)}$, are given by

$$L_{mn(q)}^{(j)} = \frac{i\Delta s}{4} H_0^{(1)}(k_j d_{mn(q)})(1-\delta_{mn(q)}) + \frac{i\Delta s}{4} H_0^{(1)} \times \left(k_j \frac{\Delta s}{2e}\right) \delta_{mn(q)}, \tag{9}$$

$$N_{mn(q)}^{(j)} = \frac{i\Delta s}{4} k_j H_1^{(1)}(k_j d_{mn(q)}) \frac{D_{mn(q)}}{d_{mn(q)}}(1-\delta_{mn(q)}) + \left(\frac{1}{2} + \frac{\Delta s}{4\pi} D'_{n(q)}\right)\delta_{mn(q)}, \tag{10}$$

where

$$d_{mn(q)} = \sqrt{(X_m - X_{n(q)})^2 + (Y_m - Y_{n(q)})^2}, \tag{11}$$

$$D_{mn(q)} = -Y'_{n(q)}(X_m - X_{n(q)}) + X'_{n(q)}(Y_m - Y_{n(q)}), \tag{12}$$

$$D'_{n(q)} = X'_{n(q)} Y''_{n(q)} - X''_{n(q)} Y'_{n(q)}, \tag{13}$$

and $H_1^{(1)}(\zeta)$ is a Hankel function of the first kind and order one. The function $\delta_{mn(q)}$ represents the Kronecker delta, and Δs is the arc length between two consecutive points of any contour. In Eqs. (12) and (13), we have defined $X'_{n(q)} \equiv X'(s)|_{s=s_{n(q)}}$, $X''_{n(q)} \equiv X''(s)|_{s=s_{n(q)}}$, and so forth. Although the notation including $n(q)$ in the functions $L_{mn(q)}^{(j)}$, $N_{mn(q)}^{(j)}$ seems to be redundant, it is necessary to indicate

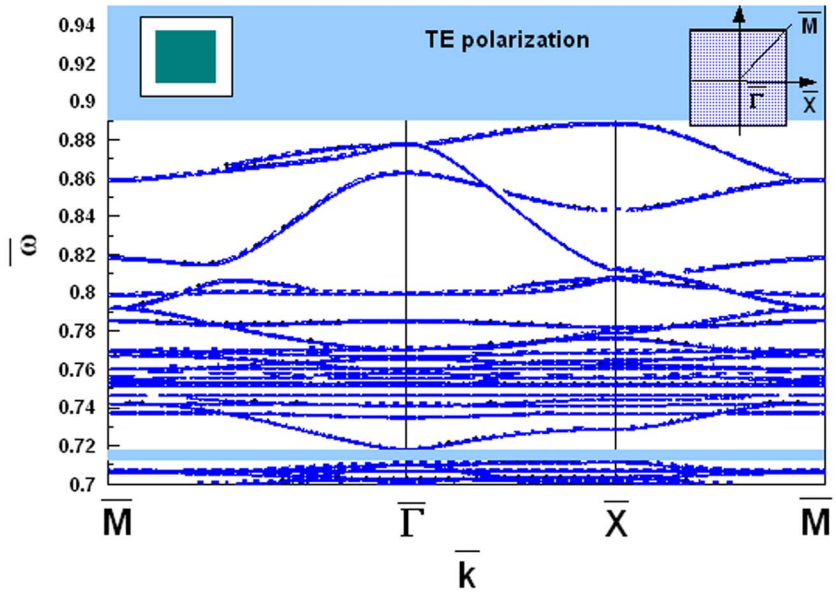

Fig. 6. (Color online) Band structure of a LR2DPC with a square Bravais lattice and square inclusions under TE polarization. The inset on the left shows the unit cell in the real space; the right inset shows the first Brillouin zone in the k space.

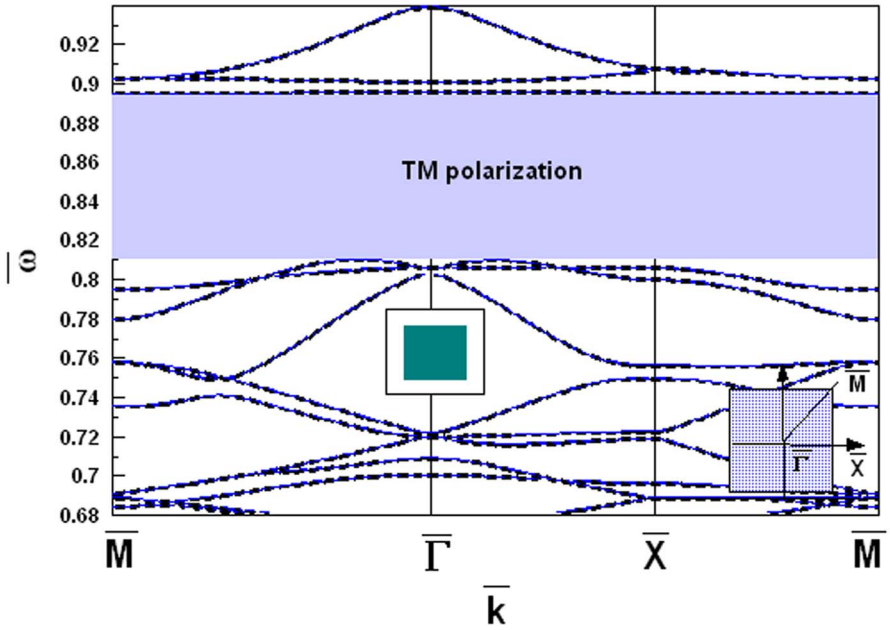

Fig. 7. (Color online) Same system as previous figure under TM polarization.

the contour where these functions will be evaluated. The boundary conditions at the contour Γ_e are

$$\Psi^{(1)}_{n(e)} = \Psi^{(2)}_{n(e)}, \quad \Phi^{(2)}_{n(e)} = \frac{f_2}{f_1}\Phi^{(1)}_{n(e)}, \tag{14}$$

where the quantity f_j is given by

$$f_j = \begin{cases} \mu_j(\omega) & \text{for TE polarization} \\ \varepsilon_j(\omega) & \text{for TM polarization} \end{cases}. \tag{15}$$

Given the translation symmetry through a LR2DPC, based on the Floquet theorem, we can state that

$$\Psi(\vec{r} + \vec{R}) = \Psi(\vec{r})e^{i\vec{K}\cdot\vec{R}}, \tag{16}$$

where $\vec{K}$ is the two-dimensional Bloch vector and $\vec{R} = D_x\hat{i} + D_y\hat{j}$ with D_x and D_y representing the unit cell dimensions. With this periodicity condition it can be shown that $\Psi^{(1)}_{n(c)} = \Psi^{(1)}_{n(a)}e^{iK_xD_x}$, $\Phi^{(1)}_{n(c)} = -\Phi^{(1)}_{n(a)}e^{iK_xD_x}$, $\Psi^{(1)}_{n(d)} = \Psi^{(1)}_{n(b)}e^{iK_yD_y}$, and $\Phi^{(1)}_{n(d)} = -\Phi^{(1)}_{n(b)}e^{iK_yD_y}$. It is worth mentioning that the sign on the normal derivatives is opposite because the normal to corresponding contours are in the opposite direction (Fig. 1).

We can use the conditions given by Eqs. (14) and the periodicity conditions to obtain a set of $2N_a + 2N_b + 2N_e$ homogeneous algebraic equations (the periodicity conditions require that $N_c = N_a$ and $N_b = N_d$).

For the region R_1 (with μ_1 and ε_1) we have

$$\sum_{n=1}^{N_a} (N^{(1)}_{mn(a)} + e^{iK_xD_x}N^{(1)}_{mn(c)})\Psi^{(1)}_{n(a)} + \sum_{n=1}^{N_a} (-L^{(1)}_{mn(a)} + e^{iK_xD_x}L^{(1)}_{mn(c)})\Phi^{(1)}_{n(a)} + \sum_{n=1}^{N_b} (N^{(1)}_{mn(b)} + e^{iK_yD_y}N^{(1)}_{mn(d)})\Psi^{(1)}_{n(b)} + \sum_{n=1}^{N_b} (-L^{(1)}_{mn(b)} + e^{iK_yD_y}L^{(1)}_{mn(d)})\Phi^{(1)}_{n(b)} + \sum_{n=1}^{N_e} N^{(1)}_{mn(e)}\Psi^{(1)}_{n(e)}$$

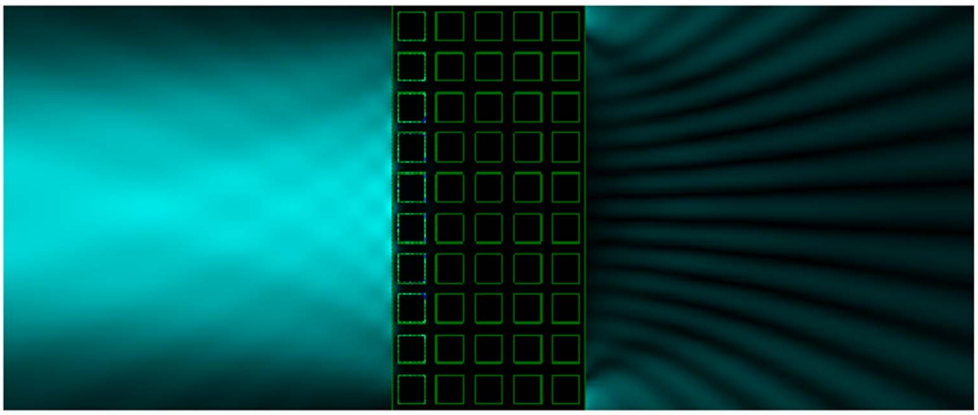

Fig. 8. (Color online) Magnetic field intensity distribution at the reduced frequency of $\bar{\omega} = 0.87$ located within the first bandgap. The region outside the LR2DPC corresponds to a near field (10 D). The incident beam goes from the left to the right. In this case the amplitude of the field in the transmission region has been amplified by a factor of an order of 10^9 to get a visible pattern.

$$-\sum_{n=1}^{N_e} L^{(1)}_{mn(e)}\Phi^{(1)}_{n(e)} = 0, \tag{17}$$

where, as it was previously stated, $m=1,2,\ldots,N_p$ for $p=a,b,\ldots,e$. For the region R_2 we have

$$\frac{f_2}{f_1}\sum_{n=1}^{N_e} L^{(2)}_{mn(e)}\Phi^{(1)}_{n(e)} + \sum_{n=1}^{N_e}(\delta_{mn(e)} - N^{(2)}_{mn(e)})\Psi^{(1)}_{n(e)} = 0, \tag{18}$$

remembering that in this case $m=1, 2,\ldots,N_e$. So, these last two equations give a system of $2N_a+2N_c+2N_e$ equations.

It is worth mentioning that different equations result when $p=a,b,\ldots,e$ and $m=1,2,\ldots,N_p$. These equations determine a square matrix M of range $2N_a+2N_b+2N_e$, whose determinant must be zero. By defining the real function,

$$D_t(k,\omega) = \ln(|\mathrm{Det}(M)|), \tag{19}$$

the singularity points of $D_t(k,\omega)$ will give us the dispersion relation $\omega=\omega(k)$, to determine the band structure.

3. ELECTROMAGNETIC FIELD DISTRIBUTION

The integral method is also suitable for calculating the electromagnetic field distribution in the near- and far-field regions of the space for a truncated finite photonic crystal (Fig. 2). Applying the Green's theorem to the vacuum incident region with an incident wave (Fig. 2), we obtain the total field [20–22]

$$\Psi(\vec{r}) = \Psi_{inc}(\vec{r}) + \frac{1}{4\pi}\int_{\Gamma_1}\left[\frac{\partial G_0(\vec{r},\vec{r}')}{\partial n_1'}\Psi_0(\vec{r}') - G_0(\vec{r},\vec{r}')\frac{\partial\Psi_0(\vec{r}')}{\partial n_1'}\right]\mathrm{d}s', \tag{20}$$

where $\Psi_{inc}(\vec{r})$ stands for the incident field and $G_0(\vec{r},\vec{r}')$ is Green's function in the vacuum region.

By considering the boundary conditions on the field and its normal derivative along the different contours Γ_p (Fig. 2), the system of equations for a finite LR2DPC can be expressed as

$$\sum_{n=1}^{N_1}[\delta_{mn(1)} - N^{(0)}_{mn(1)}]\psi^{(1)}_{n(1)} + \frac{f_0}{f_1}\sum_{n=1}^{N_1} L^{(0)}_{mn(1)}\Phi^{(1)}_{n(1)} = \psi^{inc}_m, \tag{21}$$

$$-\sum_{n=1}^{N_1} N^{(1)}_{mn(1)}\psi^{(1)}_{n(1)} + \sum_{n=1}^{N_1} L^{(1)}_{mn(1)}\Phi^{(1)}_{n(1)} - \sum_{n=1}^{N_2} N^{(1)}_{mn(2)}\psi^{(1)}_{n(2)} + \sum_{n=1}^{N_2} L^{(1)}_{mn(2)}\Phi^{(1)}_{n(2)} + \cdots - \sum_{n=1}^{N_q} N^{(1)}_{mn(q)}\psi^{(1)}_{n(q)} + \sum_{n=1}^{N_q} L^{(1)}_{mn(q)}\Phi^{(1)}_{n(q)} = 0, \tag{22}$$

$$\sum_{n=1}^{N_2}[\delta_{mn(2)} - N^{(2)}_{mn(2)}]\psi^{(1)}_{n(2)} + \frac{f_2}{f_1}\sum_{n=1}^{N_2} L^{(2)}_{mn(2)}\Phi^{(1)}_{n(2)} = 0, \tag{23}$$

$$\sum_{n=1}^{N_3}[\delta_{mn(3)} - N^{(2)}_{mn(3)}]\psi^{(1)}_{n(3)} + \frac{f_2}{f_1}\sum_{n=1}^{N_3} L^{(2)}_{mn(3)}\Phi^{(1)}_{n(3)} = 0, \tag{24}$$

$$\cdots$$

$$\sum_{n=1}^{N_{q-1}}[\delta_{mn(q-1)} - N^{(2)}_{mn(q-1)}]\psi^{(1)}_{n(q-1)} + \frac{f_2}{f_1}\sum_{n=1}^{N_{q-1}} L^{(2)}_{mn(q-1)}\Phi^{(1)}_{n(q-1)} = 0, \tag{25}$$

$$\sum_{n=1}^{N_q}[\delta_{mn(q)} - N^{(3)}_{mn(q)}]\psi^{(1)}_{n(q)} + \frac{f_3}{f_1}\sum_{n=1}^{N_q} L^{(3)}_{mn(q)}\Phi^{(1)}_{n(q)} = 0. \tag{26}$$

It is assumed in this case (see Fig. 2) that the incidence medium has the optical properties given by the magnetic permeability μ_0 and electric permittivity ε_0, the medium containing the inclusions has the properties given by μ_1,ε_1, the inclusions have the properties μ_2,ε_2, and the transmission medium's properties are given by μ_3,ε_3. Equations (21)–(26) constitute an inhomogeneous system of $2\Sigma_{p=1}^{q}N_p$ linear equations that can be solved numerically to determine the fields and their normal derivative along all the contours. Consequently the electromagnetic field at any point in the space (given by $\vec{r}$) can be determined with these contour fields by using Eq. (5) or (20) in the case that the point in question resides inside the incident region.

4. BAND STRUCTURE

The unit cell we are considering in the following discussion is composed of vacuum and a dispersive LHM whose optical properties are given by the dielectric function [18,23]

$$\varepsilon_p(\omega) = 1 - \frac{\omega_p^2}{\omega^2}, \tag{27}$$

and the magnetic permeability

$$\mu_p(\omega) = 1 - \frac{F\omega^2}{\omega^2 - \omega_0^2}. \tag{28}$$

These functions are shown in Fig. 3 with the parameters $\omega_p=10c/D$, $\omega_0=4c/D$, and $F=0.56$ [18,23]. The region where this LHM presents a negative refractive index is within the frequency range $\omega_0<\omega<\omega_{LM}$ with $\omega_{LM}=\omega_0/\sqrt{1-F}$.

In Fig. 3 and those that follow we will be using the reduced units of frequency given by $\bar{\omega}=\omega D/2\pi c$ and $\bar{k}=kD/2\pi$, where c stands for the speed of light and D is a normalization constant that we choose to be the dimension of the side of a square unit cell ($D=D_x=D_y$). In reduced units the plasma and the resonance frequencies are $\bar{\omega}_p=1.592$ and $\bar{\omega}_0=0.637$, respectively.

As a previous step to calculating the LR2DPC band structure we briefly considered the calculation of the band structure of a one-dimensional photonic crystal (LR1DPC) in order to compare the results with an analytical method [19,24]. The results are shown in Figs. 4 and 5 for the band structures (both polarizations) of a LR1DPC.

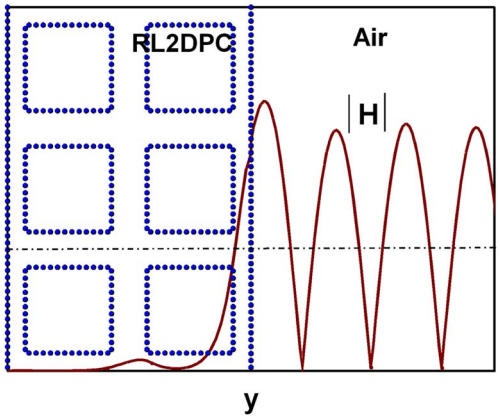

Fig. 9. (Color online) Magnitude of the magnetic field H at the line $x=0$ and the position indicated by the dashed–dotted line. At this frequency ($\bar{\omega}_0=0.87$) the field strongly decays within one period.

The band structures of a LR2DPC have similar characteristics to those of dielectric two-dimensional photonic crystals for different filling fractions. However, some interesting features appear due to the presence of LHMs. In Figs. 6 and 7 we have the band structures of a LR2DPC that has a metamaterial square inclusion with a filling fraction $f=0.5$. To determine these band structures we used the partition $\Delta s=D/20\bar{\omega}_{\min}$, with $\bar{\omega}_{\min}$ the minimum frequency of the interval shown in the corresponding graph.

A peculiar band, which is independent of the filling fraction and is due to plasmonic modes at the interface LHM vacuum, appears under TE polarization at $\bar{\omega}=0.735$ (see Fig. 6). The characteristic frequency where these modes appear can be calculated in terms of the asymptotic limit $\omega=\omega_0\sqrt{2/(2-F)}$, which results from the dispersion relation

$$|\vec{k}_{\parallel}+\vec{G}|^2=\frac{\omega^2}{c^2}\mu_1\mu_2\left(\frac{\varepsilon_2\mu_1-\varepsilon_2\mu_1}{\mu_1^2+\mu_2^2}\right), \tag{29}$$

as $|\vec{k}_{\parallel}+\vec{G}|$ goes to infinity [18,25], where $\vec{k}_{\parallel}$ represents the parallel (to Γ_1 in Fig. 2) component of the Bloch wave vector and $\vec{G}$ stands for a reciprocal lattice vector. It is evident to observe that at the limit when $\mu_2\rightarrow\mu_1$ (at the frequency where the plasmonic modes appears) each value of $\vec{G}$ in the vector $\vec{k}_{\parallel}+\vec{G}$ contributes with one band within the first Brillouin zone that is piled up around the frequency mode.

This system also presents a wide bandgap (TM polarization) within the spectral region where the inclusions have a negative refractive index. The electric field intensity distribution is shown in Fig. 8 for a Gaussian normal incident beam that is eight periods wide and has a frequency $\bar{\omega}_1=0.87$ (in the middle of the bandgap). It is worth noticing that the decaying length of the field is quite short in contrast to completely dielectric systems in spite of having small contrast in the optical properties of both media air LHM ($n_2=-0.694$) (see Fig. 9). For the calculation of field distribution we considered a partition step $\Delta s=D/20\bar{\omega}_1$. The far-field intensity as a function of the scattering angle is shown in Fig. 10. Energy conservation is a measure of the precision of the algorithm. In

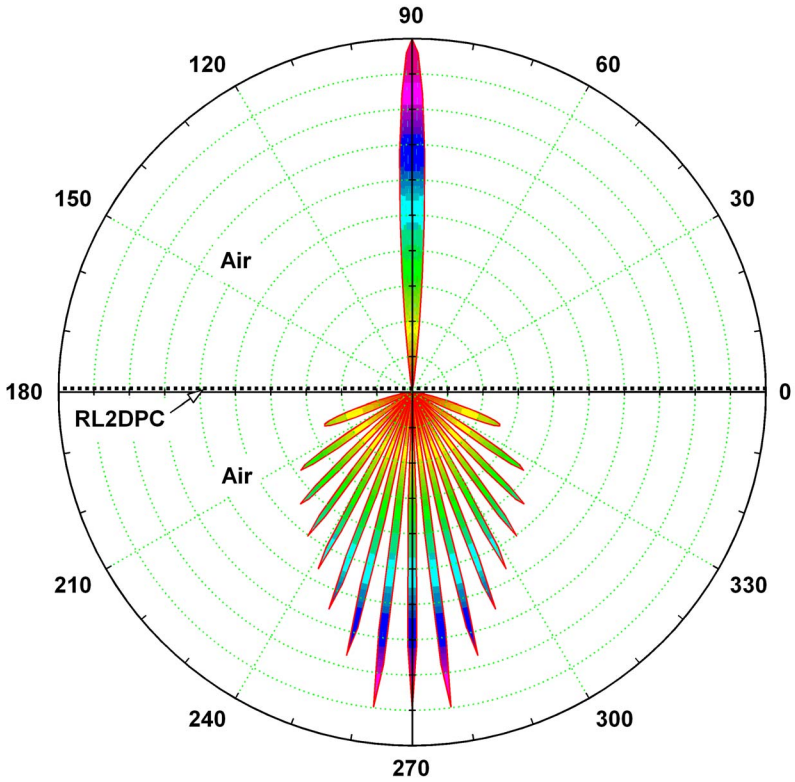

Fig. 10. (Color online) Scattered far field. The LR2DPC is in the plane $y=0$. The transmission intensity of the field (180°–360°) was amplified $\sim 10^9$ in order to make it visible on the graphic.

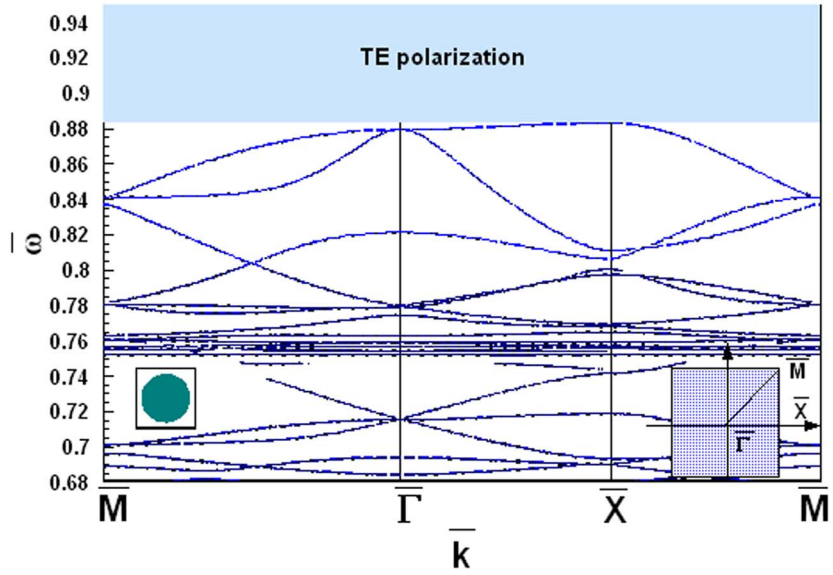

Fig. 11. (Color online) Band structure of a LR2DPC with a square Bravais lattice and circular inclusions of LHM under TE polarization.

this example, adding the reflected and transmitted energy of the scattered field, we have an error of ~2.5%, mainly from light that is lost through the lateral contours.

If we now consider a LR2DPC with circular inclusions of LHM and the same filling fraction $f=0.5$ of the previous example, the band structure is shown in Figs. 11 and 12. In this case we also have a wide bandgap in the region of high frequencies, and the peculiar band due to plasmonic modes [15,23,25] appears at the frequency $\bar{\omega}=0.754$ (TE polarization). The localization of this resonance can be clearly appreciated in Fig. 13, where we show the comparison of the determinants of both LR2DPC (with cylindrical and square inclusions) corresponding to the point $\bar{M}$ of the band structures in Figs. 6 and 11.

5. CONCLUSIONS

Dispersive left-handed materials (LHMs) of well-known properties were introduced to the structure of two-dimensional photonic crystals to study their properties. The idea of considering these systems was twofold; besides studying the band structure of LR2DPC, we tested the stability of the proposed integral method when considering dispersive materials. Some facts that deserve to be mentioned in this section are the presence of wide bandgaps where the light has a shallow penetration inside the crystal and the formation of interface bands. These plasmonic modes appear because of the presence of dielectric-LHM interfaces, which state the condition for their existence.

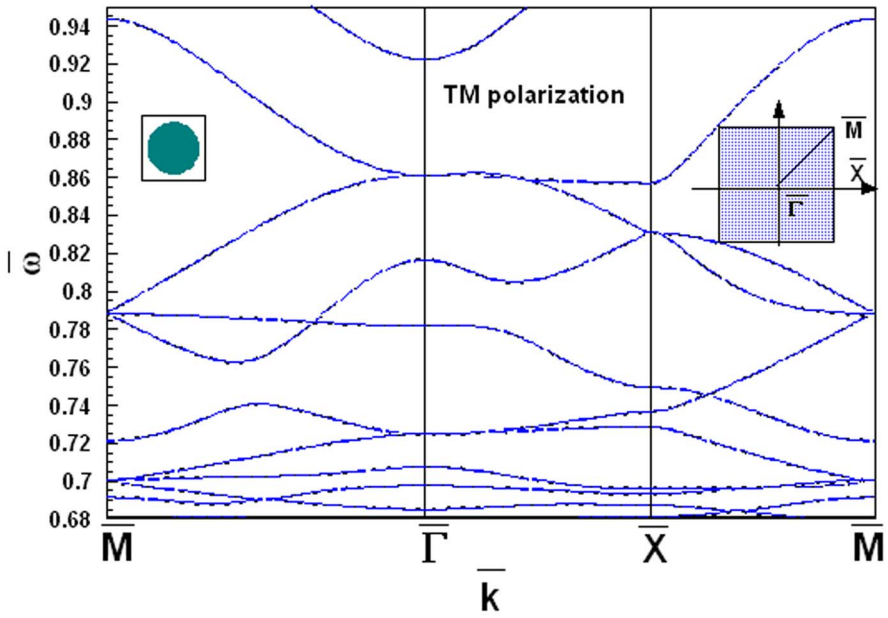

Fig. 12. (Color online) Band structure of LR2DPC under TM polarization. Same parameters as previous figure.

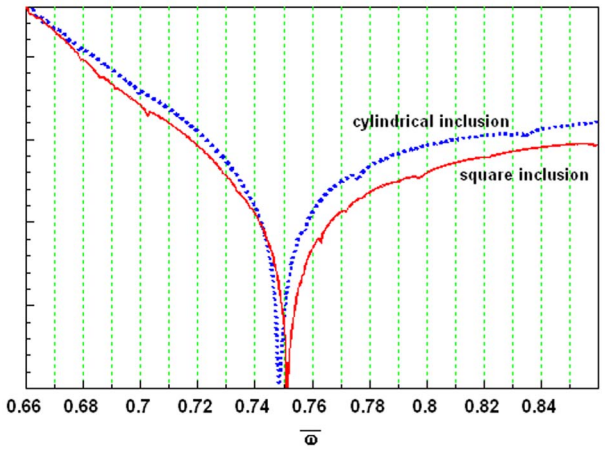

Fig. 13. (Color online) Comparison of determinants at the point $\bar{M}$ for both LR2DPCs with square and cylindrical inclusions, respectively. TE polarization.

ACKNOWLEDGMENTS

We acknowledge the valuable comments of Felipe Ramos Mendieta and the support he has provided to us through the grant given by Subsecretaría de Educación Superior e Investigación Científica, México, Programa de Mejoramiento del Profesorado, especial grant "Redes de Cuerpos Académicos 2004."

REFERENCES

1. T. Tanabe, M. Notomi, S. Mitsugi, A. Shinya, and E. Kuramochi, "Fast bistable all-optical switch and memory on a silicon photonic crystal on-chip," Opt. Lett. **30**, 2575–2577 (2005).
2. A. Femius Koenderink and W. L. Vos, "Optical properties of real photonic crystals," J. Opt. Soc. Am. B **22**, 1075–1084 (2005).
3. L. Florescu, K. Busch, and S. John, "Semiclassical theory of lasing in photonic crystals," J. Opt. Soc. Am. B **19**, 2215–2223 (2002).
4. P. Kramper, A. Birner, M. Agio, C. M. Soukoulis, F. Müller, U. Gösele, J. Mlynek, and V. Sandoghdar, "Direct spectroscopy of a deep two-dimensional photonic crystal microresonator," Phys. Rev. B **64**, 233102 (2001).
5. J. Li, W. Huang, and Y. Han, "Tunable photonic crystals by mixed liquids," Colloids Surf. **279**, 213–217 (2006).
6. T. Stomeo, V. Errico, A. Salhi, A. Passaseo, R. Cingolani, A. D'Orazio, M. De Sario, V. Marrocco, V. Petruzzelli, F. Prudenzano, and M. De Vittorio, "Design and fabrication of active and passive photonic crystal resonators," Microelectron. Eng. **83**, 1823–1825 (2006).
7. S. H. G. Teo, A. Q. Liu, M. B. Yu, and J. Singh, "Fabrication and demonstration of square lattice two-dimensional rod-type photonic band gap crystal optical intersections," Photonics Nanostruct. Fundam. Appl. **4**, 103–115 (2006).
8. M. Mengens, J. E. G. J. Wijnhoven, A. Lagendijk, and W. L. Vos, "Light sources inside photonic crystals," J. Opt. Soc. Am. B **16**, 1403–1408 (1999).
9. F. Yuntuan, S. Haijin, and S. Tinggen, "New evidences of negative refraction in photonic crystals," Opt. Mater. **28**, 1156–1159 (2006).
10. B. Momeni and A. Adibi, "Systematic design of superprism-based photonic crystal demultiplexers," IEEE J. Sel. Areas Commun. **23**, 1355–1364 (2005).
11. N. C. Panoiu, M. Bahl, and R. M. Osgood, Jr., "Optically tunable superprism effect in nonlinear photonic crystals," Opt. Lett. **28**, 2503–2505 (2003).
12. M. Soljacic, C. Luo, J. D. Joannopoulos, and S. Fan, "Nonlinear photonic crystal microdevices for optical integration," Opt. Lett. **28**, 637–639 (2005).
13. A. A. Houck, J. B. Brock, and I. L. Chuang, "Experimental observation of a left-handed material that obeys Snell's law," Phys. Rev. Lett. **90**, 137401 (2003).
14. V. A. Podolsky, "Plasmon modes and negative refraction in metal nanowire composites," Opt. Express **11**, 735–745 (2003).
15. L. Wu, S. He, and L. Chen, "On unusual narrow transmission bands for a multi-layered periodic structure containing left handed materials," Opt. Express **11**, 1283–1290 (2003).
16. L. Wu, S. He, and L. Shen, "Band structure for a one-dimensional photonic crystal containing left-handed materials," Phys. Rev. B **67**, 235103 (2003).
17. J. Li, L. Zhou, C. T. Chan, and P. Sheng, "Photonic band gap from a stack of positive and negative index materials," Phys. Rev. Lett. **90**, 083901 (2003).
18. D. Bria, B. Djafari-Rouhani, A. Akjouj, L. Dobrzynski, J. P. Vigneron, E. H. El Boudoti, and A. Nougaoui, "Band structure and omnidirectional photonic band gap in lamellar structures with left-handed materials," Phys. Rev. E **69**, 066613 (2004).
19. F. Villa-Villa and J. A. Gaspar-Armenta, "Brewster angle and optical tunneling in one-dimensional photonic crystals composed of left and right handed materials," J. Opt. Soc. Am. B **23**, 375–380 (2006).
20. A. Mendoza-Suárez, F. Villa-Villa, and J. A. Gaspar-Armenta, "Numerical method based on the solution of integral equations for the calculation of the band structure and reflectance of one and two-dimensional photonic crystals," J. Opt. Soc. Am. B **23**, 2249–2256 (2006).
21. A. A. Maradudin, E. R. Mendez, and T. Michel, "Enhanced backscattering of light from a random grating," Ann. Phys. (N.Y.) **203**, 255–307 (1990).
22. A. Mendoza-Suárez and E. R. Mendez, "Light scattering by a reentrant fractal surface," Appl. Opt. **36**, 3521–3531 (1997).
23. F. Villa, J. A. Gaspar, and A. Mendoza, "Surface modes in one dimensional photonic crystals that include left handed materials," J. Electromagn. Waves Appl. **21**, 485–489 (2007).
24. J. A. Gaspar-Armenta and F. Villa, "Band structure properties of one-dimensional photonic crystals under the formalism of equivalent systems," J. Opt. Soc. Am. B **21**, 405–412 (2004).
25. R. Ruppin, "Surface polaritons of a left-handed medium," Phys. Lett. A **227**, 61–64 (2000).